Journal of Rehabilitation in Civil Engineering 9-1 (2021) 01-18

journal homepage: http://civiljournal.semnan.ac.ir/

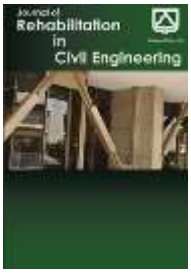

Experimental Study of Octagonal Steel Columns Filled with Plain and Fiber Concrete under the Influence of Compressive Axial Load with Eccentricity

N. Mahdavi[1], M. Salimi[1] and M. Ghalehnovi[2*]

1. M.Sc. Graduate, Department of Civil Engineering, Ferdowsi University of Mashhad
2. Associate Professor, Department of Civil Engineering, Ferdowsi University of Mashhad

Corresponding author: *Ghalehnovi@um.ac.ir*

ARTICLE INFO

Article history:
Received: 07 June 2019
Accepted: 07 April 2020

Keywords:
Load eccentricity,
Load–displacement curve,
Steel fiber reinforced concrete,
Core concrete strength.

ABSTRACT

In recent years, Concrete Filled Tube (CFT) columns have been very much taken into consideration due to the many advantages of the instrument. In experimental studies, the focus has been on compressive loading. Although in many cases the eccentric loading (the presence of a bending moment) has also been investigated, further research is needed in this regard. Therefore, in this study, the steel columns filled with concrete with a regular octagonal cross section were studied under the influence of pressure axial load with eccentricity. The parameters studied in this study include bearing capacity, coefficient of ductility and energy absorption. To test and compare the stated parameters, specimens of 150 cm height, which were filled with plain concrete and fiber reinforced concrete were tested. The compressive axial load has been applied to the specimens by the eccentricity of 50, 100 and 150 mm. The results show that at pure compressive loading, the increase in concrete core capacity increases the load bearing capacity of the specimens so that by increasing the concrete compressive strength by 50%, the bearing capacity of the cross section increases by about 15%. Also, based on the results, the average ductility coefficient for specimens was 7.4, and it seems that this value is independent of the type of loading. The use of concrete with intermediate grade resistance can increase the energy absorbed. However, according to the results, it seems that by increasing the bending moment the positive effects of the concrete core are greatly reduced.

1. Introduction

Concrete and steel are materials that are used extensively in construction. Concrete is a

DOI: 10.22075/JRCE.2020.17989.1345

brittle material, relatively inexpensive and has a significant fire resistance. Steel is also a material with high ductility and high strength. However, the use of steel only in the construction of columns, especially in high structures, is non-economic.

Composite columns are generally divided into two groups:

(A) Steel sections enclosed in concrete, also referred to as Steel Reinforced Concrete, and are referred to as SRCs.

B) Concrete filled tube which referred to CFT.

Examples of these sections are given in Fig. 1.

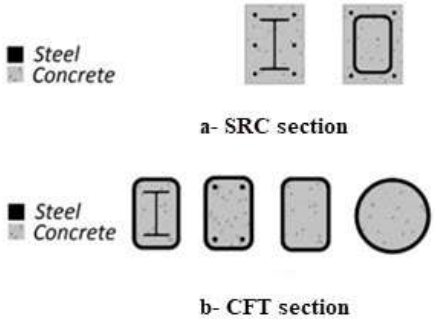

Fig. 1. Examples of composite columns.

Since the mid-twentieth century onwards, many scholars have worked on the behavior of these sections in different situations.

Gopal tested the behavior of a thin, circular column of hollow steel filled with fiber concrete under the influence of eccentric loading [1]. In this study, slenderness was considered as the main parameter and the results were shown as load-displacement curves and load-strain curves. Lotfollahi Yaghein and Ziyaeioun [2], by examining the behavior of the two-layered composite columns under the interaction of axial force and bending moment, showed that in the two-layered composite columns, with the increase in slenderness, the amount of bearing capacity is reduced, and for smaller slenderness ratios, the drop in load capacity Less, but larger for larger ratios where the column failure occurs due to the buckling phenomenon.

Tokgoz [3, 4], launched a different investigation on composite columns made of plain steel and stainless steel, which was filled with plain and fiber reinforced concrete, was subjected to two axial bending and axial compressive loading, and also investigated the effect of the main test parameters included concrete compressive strength, cross-sectional area , eccentricity, the steel fibers, and the slenderness on the structural performance of the CFT columns, and showed the bearing capacity and the load-displacement load-strain relationship.

Chang et al [5] presented a numerical analysis on CFT columns filled with steel fiber under cyclic loading and stated that the addition of steel fibers to CFT columns increases the hardness, the maximum peripheral load and the ability to deform.

In 2014, Kheyroddin et al. [6] Presented a model for circular short CFT columns using artificial neural networks.

Also first designing principles for elliptical sections based on euro code regulations for circular ones, were presented by Jamaluddin et al. [7] by conducting experimental investigations on 26 elliptical CFT specimens with variable section dimension and length.

Lu et al. [8] had an experimental investigation on 36 CFT specimen made of FRC core to evaluate failure mode, bearing capacity, ductility and hysteresis loops pinching.

Ding et al. investigated the mechanical behavior of CFT columns with circular and square cross sections. This study includes experimental and numerical investigations. A total of 20 samples were tested. Following this research, a finite element model is also performed. At the end of this study, an analytical relation for bearing capacity calculation is presented [9].

Long et al. [10] presented a validated equation for CFT sections local elastic buckling by conducting theoretical principles based on buckling energy and applying eccentric load.

Elchakani et al. [11] submitted yielding and plastic slender limitation by investigating bending moment affection in an experimental and theoretical study.

Mahgub et al. [12] in 2017 investigated 12 specimens with elliptical sections and variable concrete strength and specimen height. They used self-consolidating concrete and evaluated slender coefficient affection on buckling behavior of specimens.

In 2017, Wang et al. [13] Discussed the cyclic behavior of CFT columns with longitudinal bars. In this study, 10 test specimens were made, 8 of which were reinforced by rebar. In this study, axial load was first introduced and cyclic lateral load was applied to the specimens later. In this study, factors such as axial load value and the effect of rebar spacing were investigated. According to the study, the researchers reported that rebar use increased stiffness, increased flexural load capacity, and increased energy dissipation potential.

In 2018, Ahmadi et al. [14] presented a model using artificial intelligence to obtain the bearing capacity of thin, non-compact CFT columns.

In 2019, Lin and Zhao [15] explored the finite elements method on CFT columns. Previous research has focused on sections less than 300 mm in diameter. In this study, the researchers have investigated the effect of dimensions on the behavior of CFT columns and have stated that with increasing the size of the cross sections the previously presented models are not sufficiently accurate. They also considered the greatest impact of increasing dimensions on the behavior of concrete, and did not consider previous models to predict enclosed concrete behavior for large-dimension CFT columns. At the end of this study, a model is presented that is said to be applicable to all dimensions.

In 2019, Wei et al. [16] Investigated the effect of diameter to thickness ratio, loading conditions, type and compressive strength of concrete on column bearing capacity using a broad database containing 491 tested specimens of circular cross-section CFT column. A method for predicting the bearing capacity of CFT columns has also been proposed using von Mises yield criterion for nonlinear steel and nonlinear regression.

In 2019, Naderpour et al.[17] Presented an innovative model to obtain the behavior of enclosed concrete columns. In this study, three methods have been developed to obtain the compressive strength of FRP-enclosed concrete.

In 2019, Haji et al.[18], In an in experimental study, reinforced the short columns using FRP and finally presented three patterns for reinforcing these columns.

1.2. Importance and Goals of Research

The widespread and growing use of CFT columns in the construction industry, the lack of transparency of the rules of the regulations and the provision of relations with a high degree of certainty, as well as the lack of attention of structural engineers to this system because of the lack of clarity of the rules of the regulations, illustrates the need for further research in this field to achieve design relationships by considering the mechanical properties and the more realistic behavior of these types of columns.

In a building, due to the presence of a large number of columns under eccentric load (such as the side columns of the building, columns next to the staircase or elevators, columns attached to asymmetric roofs), it is necessary to examine the columns under the eccentric load.

Plain concrete is acceptable in pressure but weak in tension. One of the best ways to improve concrete tensile strength is the use of steel fibers in concrete. On the other hand, in this test, the load is applied off the axis. So, it's definitely part of the column will be under tension. This causes the use of fiber concrete to be evident, but the magnitude of this improvement is not clear and should be determined by the test. According to some researchers, concrete fibers increase the ductility of the column, but this is a matter of difference; therefore, the behavior of composite columns filled with fiber concrete under the eccentric load has to be investigated.

The same desirable performance and the ever-increasing use of CFT columns have led to many analytical and experimental research. A lot of research has been done on CFT columns with circular, square and rectangular sections[19-23]. Due to the proper function of these columns, other sections such as oval, octagonal, hexagonal under different axial, flexural, lateral loads such as axial compressive load, axial compressive load with eccentricity, double axis bending, incremental alternating lateral load, the simultaneous effect of axial load and lateral load are investigated [24, 25]. Also, the performance of concrete types such as plain concrete, fiber concrete and high strength concrete to fill these columns has been investigated.

Oval, octagonal and hexagonal pillars are mainly designed by structural engineers to meet the demands of architecture. Considering the above-mentioned issues regarding the CFT columns and the necessity of examining the behavior of the columns under eccentric axial load, this study investigates the behavior of composite columns with an octagonal cross-sectional steel structure filled with plain concrete and fiber concrete under axial compressive load with and without eccentricity.

2. Materials Used and Construction of Experimental Specimens

2.1. Specification of Materials

2.1.1. Concrete

In this research, two types of plain concrete and reinforced steel fiber concrete (SFRC) have been used.

2.1.1.1. Plain Concrete

Eight Octagonal CFT columns have been constructed; four of them are filled with plain concrete. At the same time as the pillars concreting, six standard cylinders with a diameter of 150 mm and a height of 300 mm, are made of plain concrete for launching strength tests and tested for compressive

strength. Based on the results of the test, the average compression strength of the specimens was 22.8 MPa. Table 1 shows the typical mixing scheme.

Table 1. plain concrete mixing scheme.

material	Gravel	sand	cement	Water
A mount (kg/m^3)	1070	720	470	248

2.1.1.2. Fiber Concrete

One of the benefits to fiber reinforced concrete in scientific research is the increased strength of rupture, increased resistance to impact, increased energy absorption, increased resistance to fatigue, increased resistance to thermal stress and shrinkage, increased tensile strength , Increased shear and flexural strength and compressive strength and increased ductility [26].

In this experiment, fiber reinforced concrete was used to fill four columns. The steel fibers used in the Hook End are as shown in Fig. 2. The technical specifications of this fiber are the length of the fiber 50 mm, the diameter of one millimeter, the ratio of the image 50, the tensile strength of 1050 MPa.

Fig. 2. Steel fibers used in concrete.

In the following, the concrete mixing plan is shown in Table (2). Also, according to the test, the average compressive strength of the specimens is 34 MPa.

Table 2. Fiber reinforced-self compacting concrete mix design.

Material	Gravel	Sand	Cement	Water	Stone powder	VMA powder	Super lubricant	Steel Fibers
A mount (kg/m3)	1120	700	400	150	100	0.09	4	55

2.1.2. Steel Plate

Steel tube of CFT octagonal columns are made with cutting, bending and welding of steel sheets; therefore, it is necessary to perform a tensile test to determine the characteristics of the steel sheet. One-dimensional test was performed on four tensile specimens made of a thick steel plate with octagonal CFT column steel sheet, based on ASTM E8 standard [27].

Herein one of investigation objectives is determining steel and concrete composition characteristics. So just ultimate and yielding strength of steel among other mechanical characteristics is needed.

In order to obtain the yield and ultimate resistances, two steel belts in the form of a dumbbell were developed according to ASTM E8 [28] instruction and tested in the Ferdowsi University of Mashhad Materials Research Laboratory. The mechanical properties of steel are given in Table 3.

Table 3. Mechanical properties of steel used for the manufacture of specimens.

Specimens	Yield Stress (MPa)	Yield Strain	Ultimate Stress (MPa)	Ultimate Strain
First steel strap	≈240	0.019	371	0.25
Second steel strap	≈250	0.0195	354	0.215
Average	245	0.01925	362.5	0.2325

2.2. Test Specimens

In this study, eight specimens of octagonal CFT columns have been constructed. In the following, their characteristics are briefly described.

2.2.1. Specifications of the Specimens Tested

In this study eight specimens of CFT columns with octagonal cross-sectional shape are tested. The main variables of the research are the type and amount of concrete strength of the core of the CFT column filler, as well as the degree of axial load eccentricity. Finally, four of these steel tubes filled with plain concrete with a compressive strength of 22.8 MPa and four others are filled with self-consolidating fiber concrete with an average compressive strength of 34 MPa.

Due to the limitation of the laboratory pressure jacks and the high capacity of the CFT columns, the process of trial and error has reached the appropriate dimensions to perform the test and the endpoint of the capacity has been estimated in this way too.

Figure 3 shows the cross-sectional shape with its nominal values.

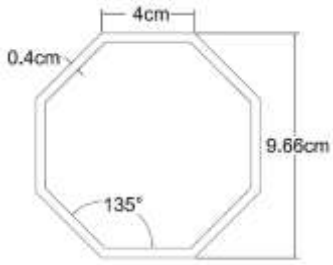

Fig. 3. Nominal dimensions of column section.

The two variable parameters in this research are one concrete core resistance and the other is the amount of eccentricity. Generally, they use a central exit to apply the moment in the lab. Here, with the amount of eccentricity of 50, 150 and 150 mm, and also axial load without eccentricity. Figure 4 shows schematically how to apply eccentricity. For this purpose, two high-rigid steel plates with a thickness of 45 mm were used. One of these sheets is mounted on the surface of the specimen to ensure that the load apply to steel and concrete core simultaneously, allowing for the development of eccentricity.

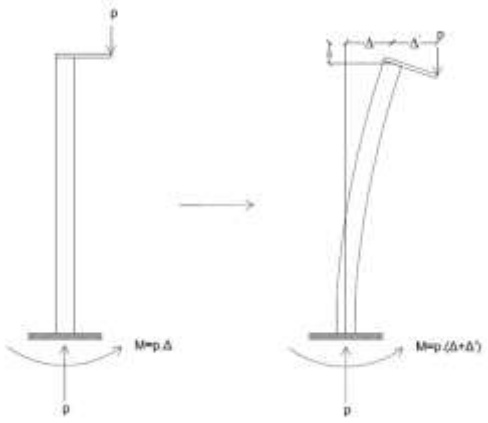

Fig. 4. A schematic illustration of the axial load with eccentricity.

2.2.2. Naming Specimens

The names of the specimens are composed of three parts. The first part means a composite column with an octagonal steel tube filled with concrete and is represented by O (Octagonal Concrete Filled Tube). The second part expresses the type of concrete that is used for the core which is P for columns filled with plain concrete and S for those filled with steel reinforced concrete. Finally, the third part indicates the amount of eccentricity of the load In cm. For example, the OP-e10 implies a composite column with an octagonal steel tube filled with plain concrete under load with the amount of eccentricity of 100mm. Further, the specimen specification is presented in Table (4). In this table, L is the length of the column, B is the length of each face of the occipital tube, t is the thickness of the steel tube, fc is the compressive strength of the concrete core, and e is the amount of eccentricity.

Table 4. Specimens Specifications.

Specimen	L×B×t (cm)	$f_c^{'}(MPa)$	e (cm)
OP-0	150×4×.4	22.8	0
OP-5	150×4×.4	22.8	5
OP-10	150×4×.4	22.8	10
OP-15	150×4×.4	22.8	15
OS-0	150×4×.4	34	0
OS-5	150×4×.4	34	5
OS-10	150×4×.4	34	10
OS-15	150×4×.4	34	15

2.3.4. Loading and Displacement Gauges Situation (Loading System)

Eccentric compressive load, applied on specimens. Eccentricity induces additional bending moment. Considered eccentricity levels are reported in table 5.

Table 5. Applied load eccentricity.

Parameters	Fiber reinforced concrete specimen				Plain concrete specimen			
Specimen number	1	2	3	4	1	2	3	4
Eccentricity (mm)	0	50	100	150	0	50	100	150

A compressive jack with 100 tonf nominal capacity has been used (the oil induces intended force). A 50 tonf load cell recorded results. Axial displacement is recorded by ultrasonic sensors and an electronical - mechanical linear variable differential transformer (LVDT) has been used to record lateral displacement. A data logger recorded displacement and induced force data. Figures 5-9 show test instruments.

Fig. 5. ultrasonic sensor.

Fig. 6. 50 tonf weight load cell.

Fig. 7. data logger.

Test accuracy depends on displacement gauges and induced load arrangement. Loading system consists of displacement gauges arrangement, applied load and recording instruments. Eccentricity induces lateral displacement so one of gauges has been conducted to record it.

Fig. 8. electro mechanical LVDT

Fig. 9. 100 tonf nominal capacity jack

The loading system is schematically shown in Figure 10. The actual loading system is also shown in Figure 11

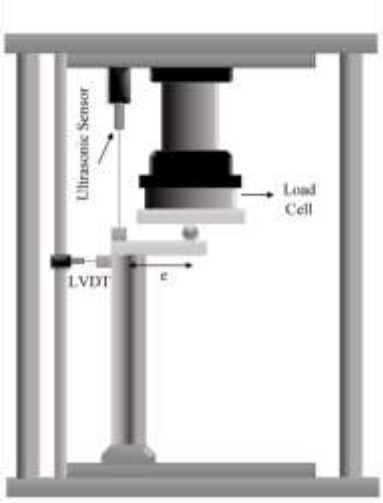

Fig. 10. schematic loading system.

Fig. 11. applying load specimen.

3. Results of Test

3.1. Load-Displacement Curve

In this study, the Load-displacement curve is used to evaluation the column's behavior.

3.1.1. Load-Displacement Curves of Specimens Filled with Simple Concrete

In Figures 12 and 13, the force-displacement diagrams from the experiment is presented for simple specimens. Considering the support conditions considered for the test specimens and the freedom of the one end of the columns, in addition to the force and axial displacement, the lateral displacement was measured at the free end of the specimen. It should be noted that theoretically, in cases of pure axial load, there is no lateral displacement until the buckling occurs, but in practice, since the load cannot be applied precisely at the center of the specimen surface, from the very beginning, the lateral displacement are happening a little, and when there is buckling, larger displacements will occur, but in the cases with eccentricity, due to the bending moment, a lateral displacement occurs from the beginning as well as the axial displacement. In the following, the force-axial and lateral displacements of specimens filled with plain concrete are presented. Loading of specimens has continued until they reach the final strength, and then the loss of strength has continued until the failure of specimens.

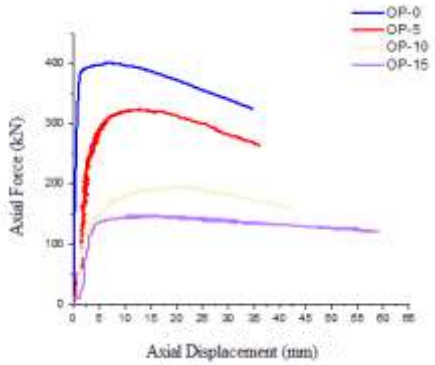

Fig. 12. Load-axial displacement diagrams of specimens filled with plain concrete.

According to the presented diagrams, it is evident that the load bearing capacity of the specimen under load without eccentricity (pure axial load) is greater than the other specimens. The axial displacement and also the lateral displacement of this specimen, especially before the specimens reach the maximum load, are clearly less than other specimens. After reaching the maximum allowable force, this specimen enters the

downward slope with a relatively large slope and its resistance decreases rapidly and results in very large displacements.

In the op-5 specimen, which is loaded at the eccentricity of 5 cm, since the eccentricity is relatively low, the behavior and shape of the diagram are close to the specimen under load without eccentricity, and the specimen enters to the downward part with slight difference in gradient with the specimen under pure axial load. This specimen experiences more displacement from the beginning than the specimen without eccentricity. Due to the moment, the amount of specimen load capacity has been reduced; that is, part of the cross-sectional capacity uses to tolerate the applied moment therefore the maximum allowable axial load has decreased relative to the specimen under the pure compressive load.

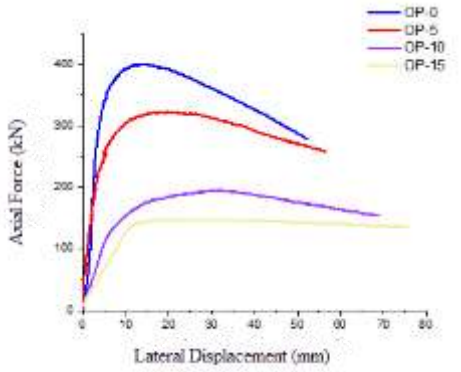

Fig. 13. Load-lateral displacement diagrams of specimens filled with plain concrete.

Fig. 14. Failing mode of specimens filled with plain concrete.

In specimens with eccentricity of 10 and 15 centimeters by increasing of the moment, the moment contribution increased in case of failure of the specimens. These specimens tolerate larger axial and lateral displacements than the other two, and in fact, before reaching the maximum allowable load, their displacement clearly is steadily increasing, and after reaching the load capacity, unlike the other two with a gentle slope and almost horizontally shifting axle and lateral displacement with a high rate of change. The existence of this bending moment reduces the bearing capacity of these specimens to a considerable extent.

In general, it can be said that during the initial loading process, the specimens are in an elastic state, which is determined by the linear section of the force-displacement diagram. The elastic axial displacement of the specimens is very small, but after the load reaches the maximum allowable force (bearing capacity) of the specimens, the bearing capacity of the specimens suddenly decreases, while the axial and lateral displacements of the specimens are increasing. It should be noted that, after reaching the specimens to the final load, there was no local buckling in the steel tube.

So far, a brief description of the load-displacement diagrams as well as the behavior of specimens filled with plain concrete has been presented.

The maximum tolerated load of specimens, the axial and lateral displacement corresponding to the maximum allowable load, as well as the percentage reduction in the load bearing capacity of the specimens, are compared with the specimen without eccentricity in Table 6. It is worth noting that

the maximum allowable force is known by the specimens as bearing capacity.

As can be seen from the results of the table, the axial load capacity decreases with the increase of the load eccentricity and hence the increase of the bending moment. Also, due to the lower lateral hardness of the specimens compared to their axial hardness, the speed of increasing lateral displacement in all specimens is greater than their axial displacement. It is noteworthy that axial and lateral displacement at the maximum load moment, for specimen OP-e15, is less than the OP-e10 specimen. This is probably due to the large increase in bending moment and a significant reduction in the load bearing capacity of the specimens.

Table 6. Bearing capacity and displacement of specimens filled with plain concrete.

Specimen	Maximum Load (kN)	Axial displacement (mm)	Lateral displacement (mm)	Strength drop to specimen with pure pressure load (%)
OP-0	401.1	6.6	13.8	0
OP-5	323.6	13.1	19.7	19.4
OP-10	195.5	21.2	32.3	51.3
OP-15	147.8	10.8	21	63.2

3.1.2 The Load-Displacement Curve of the Specimens Filled with Steel Fiber Reinforced Concrete

In the previous section, the graphs and the results of the specimens filled with plain concrete have been introduced. This section is very similar to the previous one. The following graphs and tables are presented for specimens filled with fiber concrete. The explanations given for plain concrete specimens are generally true for specimens filled with fiber concrete, and this section refuses to provide duplicate explanations. Figures ۱۵ and ۱۶ show force-displacement diagrams for specimens filled with fiber concrete.

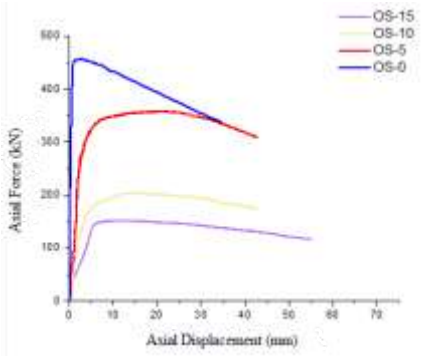

Fig. 15. Load-axial displacement diagrams of specimens filled with fiber reinforced concrete.

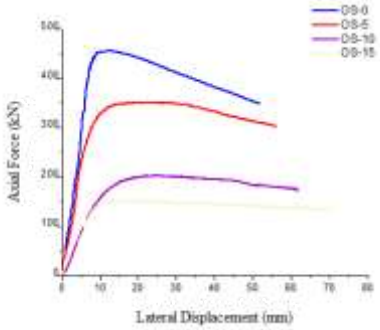

Fig. 16. Load-lateral displacement diagrams of specimens filled with fiber reinforced concrete

In the following, similar to that for specimens filled with plain concrete, for specimens filled with fiber concrete, see Table 7.

Table 7. Bearing capacity and displacement of specimens filled with fiber reinforced concrete.

Specimen	Maximum Load (kN)	Axial displacement (mm)	Lateral displacement (mm)	Strength drop to specimen with pure pressure load (%)
OS-0	457.3	2.5	12.2	0
OS-5	358.8	21.6	26.2	21.5
OS-10	204.5	9.9	22.9	55.3
OS-15	152.3	11.9	15.8	66.7

3.2. Calculate the Ductility and Energy Absorption of Specimens

As it is known, the force-displacement diagrams obtained are curvature and the calculation of the index of ductility is not possible; therefore, it is necessary to approximate the results of the diagrams in a bilinear behavior. For the approximation of the force-lateral displacement diagram, the guidance provided in 360 Journal of Management and Planning Organization [29] has been used. In clause 3-3-3-1-4 of this guidance, this bilinear behavior equation statement is based on the force diagram of the system's actual displacement as described below:

Nonlinear behavior of the structure, which identifies the relationship between the base shear and the control point displacement in accordance with Fig. 17 and 18, should be replaced by a simple bilinear behavior model in order to calculate the effective lateral force (K_e) and effective yielding shear (V_y). To simplify the nonlinear behavior model, the point B must be chosen so that the area below the bilinear behavior model is equal to the surface below the nonlinear behavior curve and also the length of the AD segment is 0/6AB. In this case, the force corresponding to point B will be the effective yielding shear (V_y) And for the $0/6V_y$ base shear in the nonlinear behavior curve, the secant modulus indicates the effective lateral force (K_e) .In the simplified model, it should be noted that V_y is not greater than the maximum of the base shear in the nonlinear behavior curve. In structures that have positive hardness after yielding, the behavior is in accordance with Fig. 1۷, and in structures that have a negative hardness after yielding, the behavior model is in accordance with Fig. 18 [29].

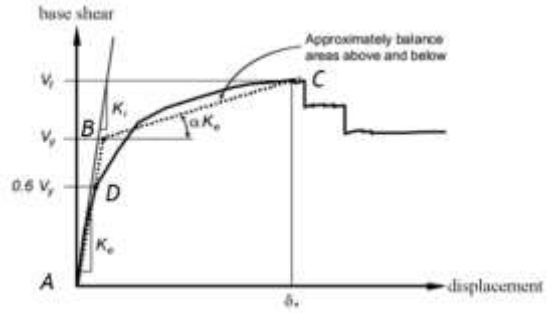

Fig. 3. Simplified diagram of force-displacement for $\alpha > 0$ [29].

It is necessary to explain that the subjects stated is for the lateral load, but the above-mentioned cases are fully exhaustive. Energy absorption and ductility coefficients are more related to lateral forces or loading that cause lateral displacement, as in the case of moment application, and therefore in this study, these parameters are calculated and compared for specimens under load with eccentricity. Subsequently, the specimens were studied separately.

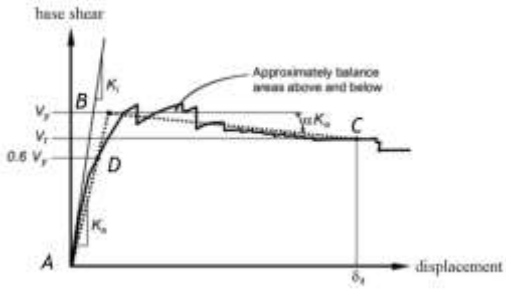

Fig. 4. Simplified diagram of force-displacement for $\alpha < 0$ [29].

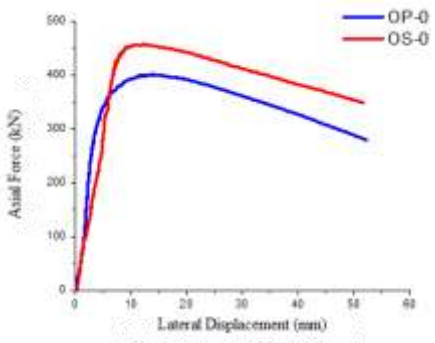

Fig. 19. Comparison between specimens with no eccentricity.

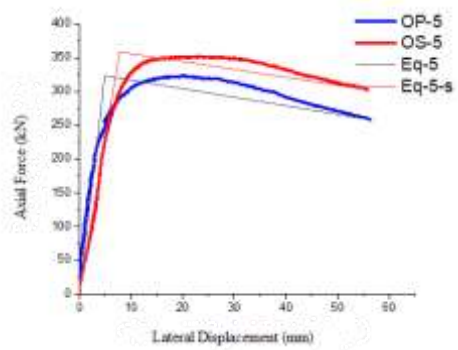

Fig. 20. comparison between specimens with 5 cm eccentricity.

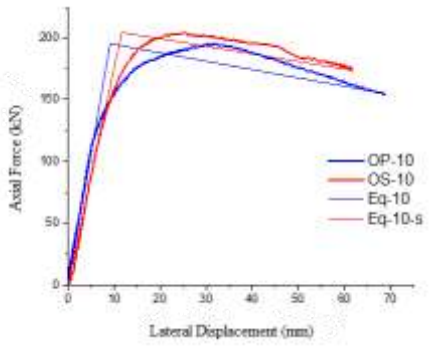

Fig. 21. comparison between specimens with 10 cm eccentricity.

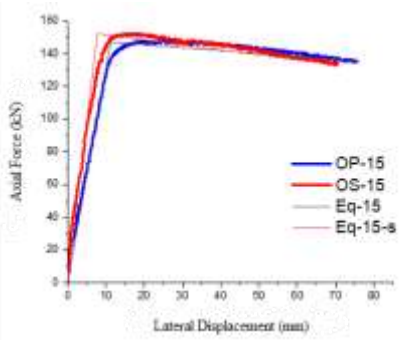

Fig. 22. Comparison between specimens with 15 cm.

In this section, the ductility of the specimens will be discussed. The most accepted equation for measuring ductility is relation (1) which is used in this study.

$$\mu = \frac{\Delta_u}{\Delta_y} \qquad (1)$$

In equation (1), Δ_y and Δ_u, are the displacements corresponding to the yield stress and the final stress respectively. Further, the calculations performed for the specimens are given in Table (7).

It should be noted that bilinear graphs have been used to compute the index of ductility because the yield point must be specified to calculate the coefficient of ductility.

As can be seen from the results of Table 8, for all specimens, the coefficient of ductility is almost the same. In fact, the effective factor in ductility seems to depend only on steel, and concrete does not play a role in ductility.

Based on the basic theory of structures, the area below the force-displacement diagram determines the energy absorption. The energy is a Newton-meter unit, also known as the Joule unit. The energy absorption results of the specimens are presented in Table 9.

Table 8. Comparison of Specimens Ductility

Specimen	$\Delta_y(mm)$	$\Delta_u(mm)$	M	average
OP-5	6.95	56.40	8.11	
OP-10	9.17	68.80	7.50	7.47
OP-15	11.13	75.65	6.80	
OS-5	7.75	56.25	7.26	
OS-10	10.8	63.4	5.87	7.36
OS-15	7.80	69.85	8.95	

Table 9. Calculation of Absorbed energy.

Specimen	Absorbed energy (j)	Increasing the absorbed energy
OP-5	15772	-
OP-10	11330	-
OP-15	9925	-
OS-5	17310	9.5
OS-10	10654	9.9
OS-15	9450	6.6

As can be seen from the results of the table, specimens filled with fiber concrete have higher absorption capacity than specimens filled with plain concrete with the same eccentricity. Of course, according to the results of the study of the index of ductility, this seems to be due to the increase in concrete core strength and, consequently, the increase in the load capacity of the specimens. It can be said, on the basis of the studies, that the effect of using the fiber on the increase in the ductility and absorption of energy is not significant.

3.4. Comparison of Load Bearing Capacity of Specimens

In this section, the load capacity of the specimens has been compared. The results of examining the load bearing capacity of the specimens are presented in Table 10.

As can be seen from the diagrams and results of Table 10, by increasing the amount of compressive load eccentricity and subsequently increasing the bending moment, the load bearing capacity of the specimens has been greatly reduced. By adding the compressive strength of the concrete core to the specimens filled with fiber concrete by 49% compared to the specimen filled with plain concrete, the load capacity for the OS-0 specimen was increased by 14%. The OS-5 increased by 10.8% as compared to the OP-5 ,the OS-10 increased by 6.4% as compared to the OP-10 and The OS-15 increased by only 3% as compared to the OP-15; Therefore, it can be said that with the increase of axial compressive load eccentricity, the effect of the compressive strength of the concrete core on the bearing capacity of the column is reduced. In fact, with the increase of bending moment and tension development in a large part of the cross section, concrete core lost its efficiency and steel plays a major role in bearing Capacity. In the form shown in Fig. 23, it is referenced in the form of bar graphs.

It should also be noted that in the case of loading without eccentricity, the effect of steel tube confinement increases concrete strength, but with part of the cross section being stretched, the steel confinement effect disappears and no increase is observed in concrete resistance. This also reduces the resistance of the specimens in the case of load without eccentricity. It should be noted that in the case of eccentric load, part of the cross-section capacity is used to endure bending moment and therefore the reduction of the cross section bearing capacity was predictable.

Table 10. Comparison between specimens bearing capacity.

Specimen	Compressive strength of concrete core (MPa)	Amount of increase in compressive strength of concrete core (%)	Maximum Load Tolerance (kN)	A mount of increase in maximum load (%)
OP-0	22.80	-	401.10	-
OP-5	22.80	-	322.60	-
OP-10	22.80	-	195.50	-
OP-15	22.80	-	147.80	-
OS-0	34.00	49.00	457.30	14.00
OS-5	34.00	49.00	358.80	10.80
OS-10	34.00	49.00	204.50	4.60
OS-15	34.00	49.00	152.30	3.00

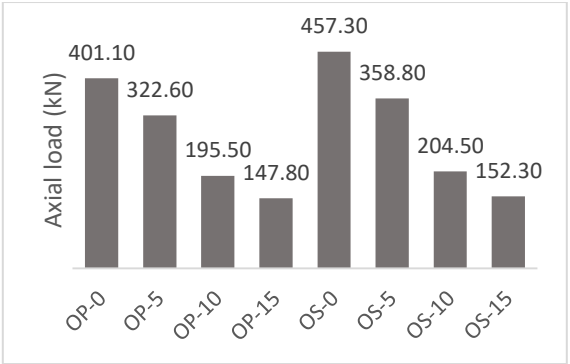

Fig. 23. Comparison between specimens bearing capacity.

3.5. Comparison of the Results of the Load Bearing Capacity of the Test with the Load Bearing Capacity Obtained in Accordance with the Steel Structures Design Regulations

The tenth chapter of the national regulations[30] has been devoted to the design of composite members, including members of steel entangled in concrete and steel members filled with concrete. The relations provided for the Regulations are general and apply for most sections. The rules of procedure have provided more relationships for steel sections filled with concrete with a circular and rectangular cross section, but engineering judgment allows us to predict parameters that are dependent on the cross-sectional shape. With the help of the Regulations, the load bearing capacity of the specimens can be obtained both in pure compression and under bending moment. For this purpose, the relationships provided in clauses 10-2-8-2-2, 10-2-8-2-2, 10-2-8-2 and 10-2-8-3-5, as well as the 10- 2-8-1 and 10-2-8-2 tables has been used[30]. In table 11, the design results are summarized in accordance with the rules of the regulations and for the pure pressure load. In this table, P_n is the nominal compressive strength of the cross section and P_u is the design compressive strength of the section according to the tenth chapter of the national regulations.

Table 11. Design compressive strength of specimens according to the tenth chapter of the national building regulations (Design and Construction of Steel Structures).

Specimen	P_n (N)	P_u (N)
with plain concrete	288900	216670
with fiber concrete	319610	239710

Also, in Table 12, a summary of the survey done for the bending strength of the specimen section is presented in accordance with the regulations. In this table, y_p specifies a neutral plastic axle, Mn is the nominal sectional strength and Mu is a cross-sectional bending strength.

Table 5. Bending capacity of specimens according to the tenth chapter of the national building regulations (Design and Construction of Steel Structures).

Specimen	y_p (cm)	M_n (N-m)	M_u (N-m)
with plain concrete	3.03	10918	9826.2
with fiber concrete	2.77	10991.2	9892.1

Table 6. Comparison of bearing capacity between test specimens and calculations according to the tenth chapter of the national building regulations (Design and Construction of Steel Structures).

Specimens	Bearing capacity obtained from the test (kN)	Bearing capacity of based on the Iran Design code (kN)	Difference percentage
OP-0	401.1	260	35
OP-5	323.6	119.5	63
OP-10	195.5	77.6	60
OP-16	147.8	54.6	63
OS-0	457.3	287.7	37
OS-5	358.8	125.5	65
OS-10	204.5	80.3	61
OS-16	152.3	56.1	63

In the following, the final capacity of the design of the specimens, taking into account the combination of compressive force and bending moment, is calculated based on the relationships of the tenth chapter of the national regulations of Iran. Also, the load capacity of the specimens obtained from the test and the percentage reduction in the

values of the regulations relative to the results of the test, are presented in Table 13 and compared.

As it is clear, the difference between the results obtained from the codes and the tests is very high. At least two parameters appear to play a direct role in this difference. The first parameter that can have a significant impact on the results is the difference in steel behavior in the code and in reality. The code considers steel behavior as two-line and considers the maximum stress equal to the yield stress, but according to Table 2, it is clear that the average stress for steel is about 1.48 times its average yield stress. The second parameter that may point to the difference in results is the discussion of how to consider the bending moment- axial force interaction. CFT columns act like reinforced concrete columns, meaning the compressive axial load and bending moment influence each other. The bending moment- axial force curve is required to consider this interaction, but a different approach has been adopted in the steel structure code. In the Code, the tolerable bending moment value is calculated based on cross section specifications, regardless of the compressive load. Also, the control equation proposed to consider the simultaneous effect of compressive load and bending moment provided in section 10-2-7-2-1 does not take into account the load interaction [23]. In fact, the values of compressive load and bending moment are compared separately with the permissible values. This view seems to be somewhat conservative. It is also worth noting that in addition to the above, the resistance coefficients also increase the difference in results. A closer look at the above paragraph is discussed below and the area not covered by the Code is schematically shown in Figure 24.

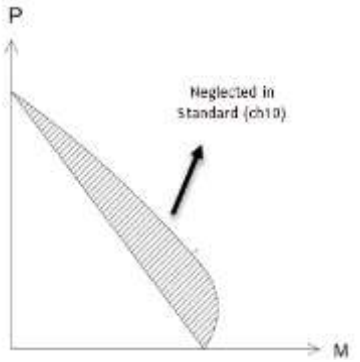

Fig. 24. Schematic of the area considered by the code and the precise area based on bending moment-compressive load interaction.

According to clause 10.2-7-2-1:

$$\frac{P_u}{P_c}+\frac{8}{9}\left(\frac{M_{u_x}}{M_{c_x}}+\frac{M_{u_y}}{M_{c_y}}\right)\le 1 \qquad (2)$$

$$P_c = c_1 \ , \ P_u = x \qquad (3)$$

$$\frac{9}{8}M_{c_x} = c_2 \ , \ M_{u_x} \qquad (4)$$

$$\rightarrow \frac{x}{c_1}+\frac{y}{c_2}=1 \qquad (5)$$

As illustrated in Fig. 24, the code acts conservatively with respect to the bending moment-axial force. Other factors mentioned also increase the discrepancy of results.

4. Conclusion

The following results are obtained by testing the octagonal CFT columns and examining what these experiments achieved.

1) With the addition of compressive strength of the concrete core, specimens filled with fiber concrete at 49%, compared to specimens filled with plain concrete, the axial bearing capacity for the specimen eccentricity was 14%, for example with an eccentricity of 50 mm, 10.8%, for example, with an eccentricity of 100 mm, 4.6%, and for example with an eccentricity of 150 mm,

increased by 3%. Based on these results, it can be stated that by increasing the moment on the cross section, the effect of the concrete core is greatly reduced. It can be stated quantitatively that in pure compressive loading, with approximately 50% increase in concrete core resistance, an increase of approximately 15% in load bearing capacity is expected; however, this value decreases with the formation and increase of the bending moment, so that in the large bending moments the bearing capacity can be unaffected of concrete core resistance.

2) Based on the studies, it seems that the coefficient of deformation is not dependent on loading, and for the sections of the test specimens, it is about 7.4. This number indicates that the test specimens can tolerate a displacement 7 times bigger than yielding displacement. This relatively high ductility index is due to the proper use of steel plastic capacity due to the absence of local buckling.

3) Increasing the strength of concrete core increases the load capacity and therefore the absorbed energy increases, as the results show that at the eccentricity of 15 cm, although the use of high strength concrete core only increases the bearing capacity of 3%, but the energy absorption to a degree Increased by 6.5%. It is also evident at the eccentricity of zero (pure pressure load) of 9.5%.

4) The improvement of side parameters, such as energy absorption and the degree of deformation due to the use of steel fibers, was not observed. In fact, the effect of concrete core on the ductility and absorption of energy is low, and therefore the addition of fibers does not significantly affect the behavior of the specimens.

5) Comparison of the results of the experiment for the octagonal sections with the dimensions indicated by the results of the Steel Structures Design Regulation of Iran (Section 10 of the National Building Regulations) shows a significant difference. Also, the difference in results increases with an increase in the moment applying the cross section.

6) According to the results, it seems that in columns with high eccentricity, the use of concrete with medium compression strength and steel fibers is not economical and does not affect the characteristics of CFT columns. This is due to an increase in the tension area due to a moment enlargement and the inability of the concrete to withstand it.

REFERENCES

[1] S.R. Gopal, P.D. Manoharan, Experimental behaviour of eccentrically loaded slender circular hollow steel columns in-filled with fibre reinforced concrete, Journal of Constructional Steel Research, 62(5) (2006) 513-520.

[2] M.L. Yaghin, M. Ziyaeioun, Analytical Study of concrete-filled double skin steel tubular columns under interaction of bending moment and axial load, journal of modeling in emgeerning, 10(31) (2013) 15-23.

[3] S. Tokgoz, Tests on plain and steel fiber concrete-filled stainless steel tubular columns, Journal of Constructional Steel Research, 114 (2015) 129-135.

[4] S. Tokgoz, C. Dundar, Experimental study on steel tubular columns in-filled with plain and steel fiber reinforced concrete, Thin-Walled Structures, 48(6) (2010) 414-422.

[5] X. Chang, Y.-Y. Wei, Y.-C. Yun, Analysis of steel-reinforced concrete-filled-steel tubular (SRCFST) columns under cyclic loading, Construction Building Materials, 28(1) (2012) 88-95.

[6] A. Kheyroddin, H. Naderpour, M. Ahmadi, Compressive strength of confined concrete in CCFST columns, Journal of Rehabilitation in Civil Engineering, 2(1) (2014) 106-113.

[7] N. Jamaluddin, D. Lam, X. Dai, J. Ye, An experimental study on elliptical concrete filled columns under axial compression, Journal of Constructional Steel Research, 87 (2013) 6-16.

[8] Y. Lu, N. Li, S. Li, H. Liang, Behavior of steel fiber reinforced concrete-filled steel tube columns under axial compression, Construction and Building Materials, 95 (2015) 74-85.

[9] F.-x. Ding, J. Liu, X.-m. Liu, Z.-w. Yu, D.-w. Li, Mechanical behavior of circular and square concrete filled steel tube stub columns under local compression, Thin-Walled Structures, 94 (2015) 155-166.

[10] Y.-L. Long, J. Wan, J. Cai, Theoretical study on local buckling of rectangular CFT columns under eccentric compression, Journal of Constructional Steel Research, 120 (2016) 70-80.

[11] M. Elchalakani, A. Karrech, M. Hassanein, B. Yang, Plastic and yield slenderness limits for circular concrete filled tubes subjected to static pure bending, Thin-Walled Structures, 109 (2016) 50-64.

[12] M. Mahgub, A. Ashour, D. Lam, X. Dai, Tests of self-compacting concrete filled elliptical steel tube columns, Thin-Walled Structures, 110 (2017) 27-34.

[13] Y.-T. Wang, J. Cai, Y.-L. Long, Hysteretic behavior of square CFT columns with binding bars, Journal of Constructional Steel Research, 131 (2017) 162-175.

[14] M. Ahmadi, H. Naderpour, A. Kheyroddin, A Proposed Model for Axial Strength Estimation of Non-compact and Slender Square CFT Columns, 43(1) (2019) 131-147.

[15] S. Lin, Y.-G. Zhao, Numerical study of the behaviors of axially loaded large-diameter CFT stub columns, Journal of Constructional Steel Research, 160 (2019) 54-66.

[16] Y. Wei, C. Jiang, Y.-F. Wu, Confinement effectiveness of circular concrete-filled steel tubular columns under axial compression, Journal of Constructional Steel Research, 158 (2019) 15-27.

[17] H. Naderpour, K. Nagai, P. Fakharian, M. Haji, Innovative models for prediction of compressive strength of FRP-confined circular reinforced concrete columns using soft computing methods, Composite Structures, 215 (2019) 69-84.

[18] M. Haji, H. Naderpour, A. Kheyroddin, Experimental study on influence of proposed FRP-strengthening techniques on RC circular short columns considering different types of damage index, Composite Structures, 209 (2019) 112-128.

[19] J. Cai, Z.-Q. He, Axial load behavior of square CFT stub column with binding bars, Journal of Constructional Steel Research, 62(5) (2006) 472-483.

[20] S.-H. Lee, B. Uy, S.-H. Kim, Y.-H. Choi, S.-M. Choi, Behavior of high-strength circular concrete-filled steel tubular (CFST) column under eccentric loading, Journal of Constructional Steel Research, 67(1) (2011) 1-13.

[21] S.-W. Liu, T.-M. Chan, S.-L. Chan, D.K.-L. So, Direct analysis of high-strength concrete-filled-tubular columns with circular & octagonal sections, Journal of Constructional Steel Research, 129 (2017) 301-314.

[22] X. Mao, Y. Xiao, Seismic behavior of confined square CFT columns, Engineering structures, 28(10) (2006) 1378-1386.

[23] X. Qu, Z. Chen, G. Sun, Experimental study of rectangular CFST columns subjected to eccentric loading, Thin-Walled Structures, 64 (2013) 83-93.

[24] F.-x. Ding, Z. Li, S. Cheng, Z.-w. Yu, Composite action of hexagonal concrete-filled steel tubular stub columns under axial loading, Thin-Walled Structures, 107 (2016) 502-513.

[25] F.-x. Ding, Z. Li, S. Cheng, Z.-w. Yu, Composite action of octagonal concrete-filled steel tubular stub columns under

axial loading, Thin-Walled Structures, 107 (2016) 453-461.

[26] J. Gao, W. Sun, K. Morino, Mechanical properties of steel fiber-reinforced, high-strength, lightweight concrete, Cement Concrete Composites, 19(4) (1997) 307-313.

[27] A. Standard, E8. Standard test method for tension testing of metallic materials, West Conshohocken : ASTM, (2004).

[28] A.S.f.T. Materials, Standard test methods for tension testing of metallic materials, ASTM international, 2016.

[29] T.C. Codification, Instruction for Seismic Rehabilitation of Existing Buildings Office of Deputy for Technical Affairs Technical Criteria Codification & Earthquake Risk Reduction Affairs Bureau ,Islamic Republic of Iran Management and Planning Organization, Tehran 2007.

[30] The tenth chapter of the national building regulations: Design and Construction of Steel Structures, Tehran, 2013.